Investigation of Mg-Bi Melts by Means of X-Ray- and Neutron Diffraction

Michael Weber, Siegfried Steeb and Peter Lamparter

Max-Planck-Institut für Metallforschung, Institut für Werkstoffwissenschaften, Stuttgart

Z. Naturforsch. **34a**, 1398–1403 (1979); received August 25, 1979

Neutron diffraction experiments were done on Mg-Bi melts with eight compositions. From the measured intensities total structure factors and pair correlation functions as well as radial atomic distribution functions were calculated. The concentration dependence of the measured nearest neighbour distance and measured coordination number indicates the preference of unlike nearest neighbours within the Mg-Bi melts.

The neutron-intensity curves show premaxima at $q \cong 1.6$ Å^{-1}. X-Ray diffraction experiments performed on melts with three different compositions also yield corresponding premaxima. It could be shown that the premaximum intensity from the X-Ray as well as from the neutron experiment corresponds to the assumption that the premaxima are caused by modulation of the monotonic Laue scattering.

1. Introduction

The structure sensitive properties of Mg-Bi melts show a very pronounced concentration dependency, as can be seen for example from Fig. 1 which shows

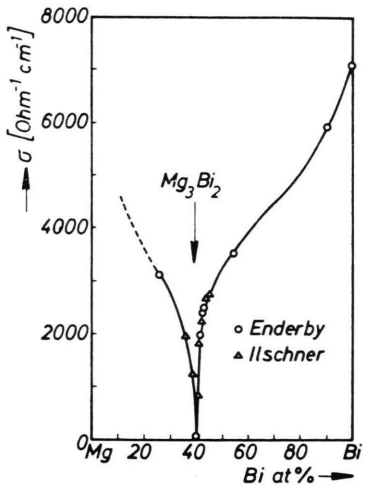

Fig. 1. Mg-Bi system: Specific electrical conductivity according to [1, 2] ($T = 900$ °C).

the electrical conductivity vs. the concentration [1, 2]. In spite of the fact that molten magnesium and molten bismuth both exhibit typical metallic behaviour, the specific conductivity of the molten alloys shows a deep minimum at the composition of the solid intermetallic compound Mg_3Bi_2.

All properties of Mg-Bi melts such as compressibility or thermodynamic activity measured up to now indicate the predominance of unlike nearest neighbours which might be caused by strong non metallic bond [3, 4]. In the present work the atomic structure of Mg-Bi melts is evaluated.

2. Theoretical Background

2.1. Intensity Functions

The intensity of the coherently scattered radiation can be written for a binary alloy in the following way [5]:

$$I_{\mathrm{coh}}(q) = \langle b^2\rangle - \langle b\rangle^2 + \langle b\rangle^2\left[1 + \int_0^\infty 4\pi r^2(\varrho(r) - \varrho_0)\cdot\frac{\sin(qr)}{qr}\,\mathrm{d}r\right] \quad (1)$$

with

$$\langle b^2\rangle = c_A b_A^2 + c_B b_B^2\,, \quad (2)$$

$$\langle b\rangle = c_A b_A + c_B b_B\,. \quad (3)$$

$\varrho(r)$ represents the local number density which depends also on the scattering lengths according to (4):

$$\varrho(r) = \frac{1}{\langle b\rangle^2}\left[c_A b_A^2\,\varrho_{AA}(r) + c_B b_B^2\,\varrho_{BB}(r) + 2\,c_A b_A b_B\,\varrho_{AB}(r)\right] \quad (4)$$

b_A, b_B = coherent scattering length of species A, B (in units of 10^{-12} cm for X-rays as well as for neutrons),

Reprint requests to Prof. Dr. S. Steeb, Max-Planck-Institut für Metallforschung, Institut für Werkstoffwissenschaften, Seestraße 92, D-7000 Stuttgart.

0340-4811 / 79 / 1200-1398 $ 01.00/0. — Please order a reprint rather than making your own copy.

q $= 4\pi \sin\theta/\lambda$,
2θ = angle between primary and diffracted beam,
λ = wavelength,
c_A, c_B = atomic fraction of species A, B ($c_A + c_B = 1$),
$\varrho_{ij}(r)$ = atomic number density of atoms of species j at a distance r from an atom of species i,
ϱ_0 $= N_L D \cdot 10^{-24}/A$ = mean atomic number density,
D = macroscopic density,
A = mean atomic weight,
N_L = Avogadro's number.

The total structure factor $S(q)$ is defined as

$$S(q) = \frac{I_{\text{coh}}(q) - [\langle b^2\rangle - \langle b\rangle^2]}{\langle b\rangle^2}. \tag{5}$$

The expression $[\langle b^2\rangle - \langle b\rangle^2]$ is designed as monotonic Laue scattering I_{LMS} which also can be expressed as

$$I_{\text{LMS}} = [\langle b^2\rangle - \langle b\rangle^2] = c_A c_B (b_A - b_B)^2. \tag{6}$$

2.2. Pair Correlation Function and Atomic Distribution Function

By Fourier transform of the structure factor $S(q)$ the pair correlation function $G(r)$ is obtained:

$$G(r) = 4\pi r(\varrho(r) - \varrho_0) \tag{7}$$
$$= \frac{2}{\pi}\int_0^\infty q(S(q) - 1)\sin(qr)\,dq.$$

The atomic distribution function

$$A(r) = rG(r) + 4\pi r^2 \varrho_0 \tag{8}$$

is used to obtain by integration the experimental coordination number N^{I}.

3. Experimental Background

3.1. Neutron Diffraction

During the present work melts from pure bismuth and from eight alloys with different concentrations were investigated. The alloys were melted within a vacuum induction furnace under argon atmosphere and casted in cylindrical molds. The specimen containers were made from pure sintered Al_2O_3 (Degussit Al-23, Fa. Degussa, Hanau) in cylindrical shape (length 100 mm, outer diameter 11 mm, wall thickness 0.5 mm). The cylinders were closed on both sides by Al_2O_3-caps using a tight, high temperature resistent cement (Fa. C. Huth, Bietigheim). These specimen containers showed no chemical reactivity with the melts, contributed a rather small background scattering, and were vacuum tight.

The neutron diffraction experiments were performed at Kernforschungszentrum Karlsruhe (FR2, Project 14, Ref. [6]). The heating device described in Ref. [7] was improved by an electronic temperature control unit. The neutron wavelength used during the experiments was 1.16 Å. The investigation of the melts was done at temperatures of about 20 °C above the corresponding liquidus temperature (for the phase diagram see [8]) using the transmission method in the angle-region $5° \leqq 2\theta \leqq 118°$ corresponding to $0.5\ \text{Å}^{-1} \leqq q \leqq 9.3\ \text{Å}^{-1}$ using a step width of $\Delta(2\theta) = 0.25°$. In the average 3000 counts/position were obtained which corresponds to a relative statistical error of 2%. For the data reduction the methods described in [7, 9] were used. The macroscopic densities needed for the evaluation were taken from [10, 11] for the melts of the pure components. For the alloys data from [12] were taken and extrapolated according to the method described in [9] to the temperature of investigation. The densities used for the evaluation are given in Table 1.

3.2. X-Ray Diffraction

The X-ray diffraction experiments in transmission were performed according to the method described in [13]. Since bismuth is a strong absorber

Table 1. Bi-Mg melts: Temperatures of investigation and densities.

Bi-concentration [at%]	Temperature of investigation T [°C]	$D(T)$ [g/cm³]
10	585	2.69
20	615	3.72
30	710	4.63
40	850	5.42
50	620	6.38
70	530	7.94
80	460	8.62
90	390	9.30
100	300	9.99

for X-rays, thin specimens were required. On the other hand, the specimens became more brittle with increasing Bi-content. Therefore the preparation, i.e. machining by rolling was only possible for Bi-contents up to 30 at% Bi.

4. Results

4.1. Neutron Diffraction

4.1.1. Intensity Curves

Fig. 2 shows the coherently scattered intensity $I_{\mathrm{coh}}(q)$. The temperatures of investigation for the specimens with different concentrations are tabulated in Table 1.

4.1.2. Pair Correlation Functions

The pair correlation functions calculated according to Eqs. (5) and (7) from the intensity curves in Fig. 2 are plotted for the different concentrations versus the interatomic distance r in Figure 3.

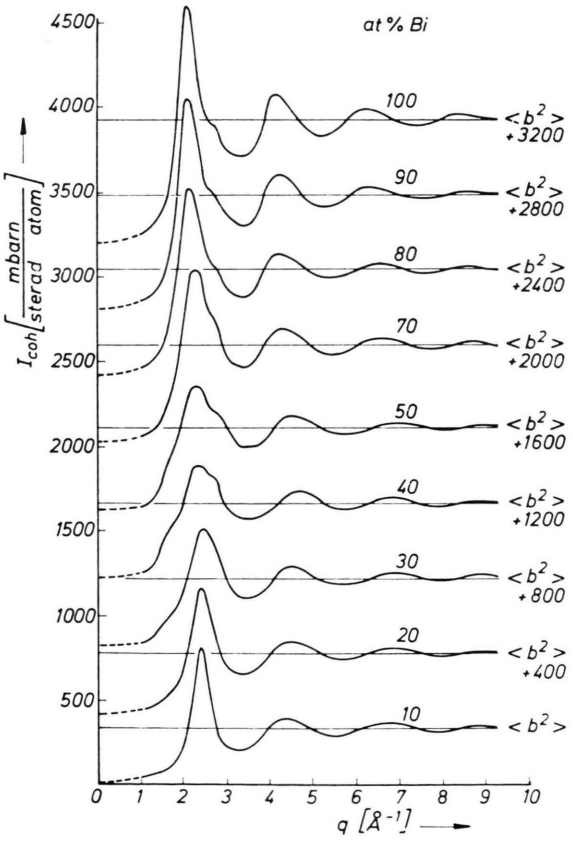

Fig. 2. Mg-Bi system: Intensity curves (neutron diffraction).

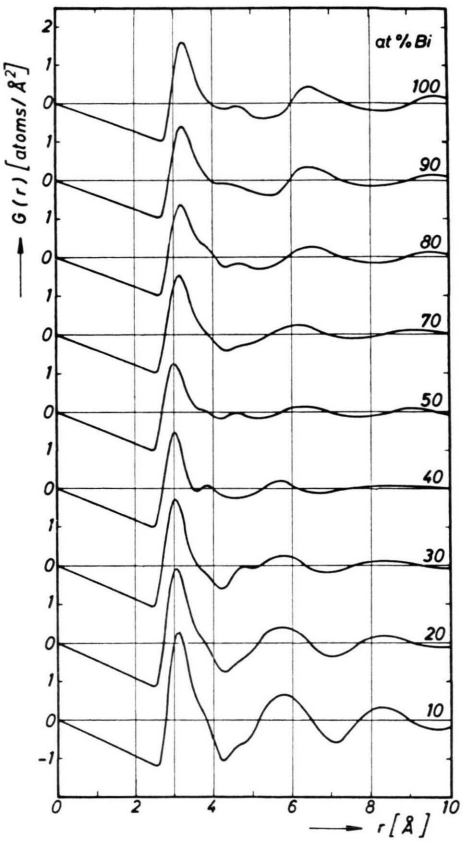

Fig. 3. Mg-Bi system: Pair correlation curves (neutron diffraction).

4.1.3. Radius r^{I} of the First Coordination Sphere

From the pair correlation functions shown in Fig. 3 the distance r^{I} of nearest neighbours was taken. Figure 4 shows the concentration dependency of this distance. The r^{I}-value for pure magnesium was taken from [14]. For all compositions r^{I} clearly lies below the curve (dashed) for a melt with statistical distribution of both kinds of atoms, which follows according to [15] from

$$r^{\mathrm{I}}_{\mathrm{St.}} = \frac{c_{\mathrm{A}}\, r^{\mathrm{I}}_{\mathrm{A}}\, b_{\mathrm{A}} + c_{\mathrm{B}}\, r^{\mathrm{I}}_{\mathrm{B}}\, b_{\mathrm{B}}}{c_{\mathrm{A}}\, b_{\mathrm{A}} + c_{\mathrm{B}}\, b_{\mathrm{B}}} \tag{9}$$

with $r^{\mathrm{I}}_{\mathrm{A,B}}$ nearest neighbour distance in the pure melt of A, B, respectively.

The minimum value of the $r^{\mathrm{I}}(c)$-curve lies at the concentration corresponding to Mg_3Bi_2.

4.1.4. Measured Coordination Number N^{I}

The area below the first maximum of the atomic distribution function $A(r)$ was determined by taking

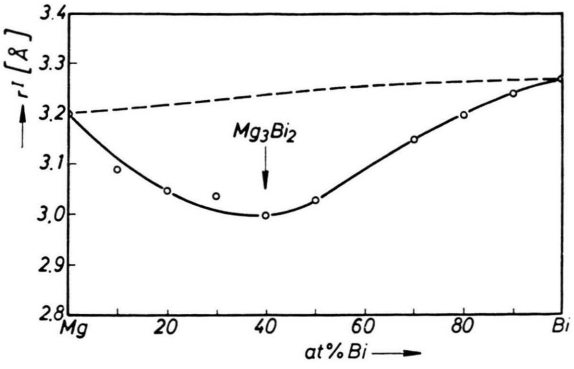

Fig. 4. Mg-Bi system: Measured radius r^I of the first coordination sphere (neutron diffraction).

twice the area of the peak in the q-region between the low q side minimum and the maximum of the main peak. This area corresponds to the measured coordination number N^I which is plotted versus the concentration in Figure 5. For all compositions N^I clearly lies below the curve (dashed) for a melt with statistical distribution, which follows from

$$N^I_{St.} = c_A N^I_A + c_B N^I_B \tag{10}$$

with $N^I_{A,B}$ coordination number in the pure melt of A, B, respectively.

As in the case of r^I, the minimum value of the $N^I(c)$-curve lies at the concentration corresponding to Mg_3Bi_2 and is rather pronounced.

4.2. X-Ray Diffraction

In Fig. 6 the coherently scattered intensities for the melts containing 10, 20, and 30 at% Bi are shown.

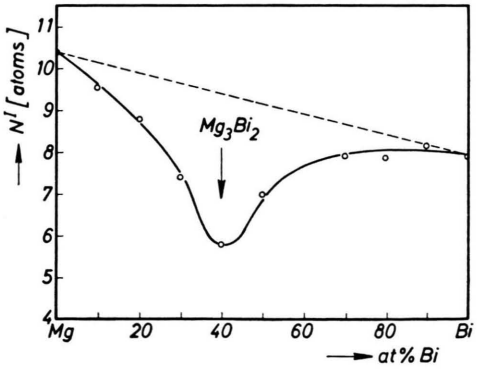

Fig. 5. Mg-Bi system: Measured coordination number N^I of the first coordination sphere (neutron diffraction).

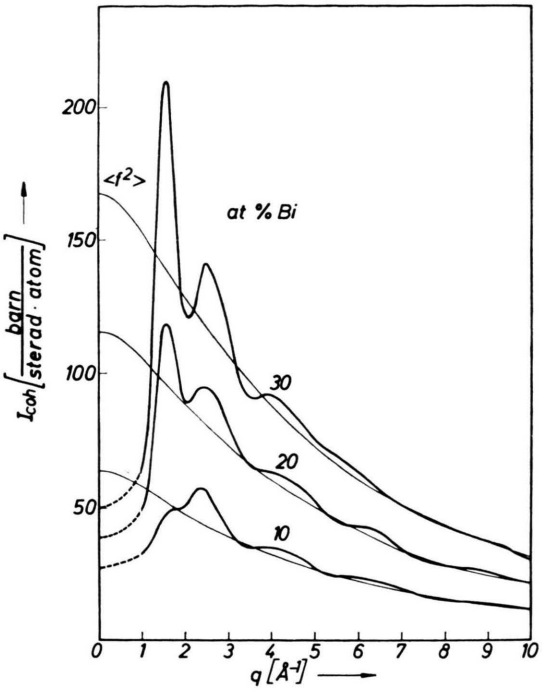

Fig. 6. Mg-Bi system: Intensity curves (X-ray diffraction).

5. Discussion

5.1. Classification of the Melts

Binary metallic melts can be classified into three types, namely melts with statistical distribution of the atoms of both species, melts with segregation tendency, and melts with tendency to compound formation. From the run of the measured coordination number N^I in Fig. 5 as well as from the run of the measured nearest neighbour distance r^I in Fig. 4 according to [16] follows that the Mg-Bi melts belong to the compound forming class. The most pronounced deviation from the statistical distribution occurs at the concentration of the corresponding solid intermetallic compound Mg_3Bi_2. In this connection one remark should be done concerning the influence of the temperature on the concentration dependency of the measured coordination number: With rising temperature the melts approach statistical distribution of the atoms of both kinds and therefore a coordination number of approximately 10. In Fig. 5 the lowest value was obtained at the highest temperature. Thus indead very strong compound forming forces must be present in these melts. The nearest neighbour distance also becomes

larger with rising temperature. In Fig. 4 the lowest value was obtained at the highest temperature, and we conclude also from this fact very strong compound forming tendency.

5.2. Interpretation of the Premaximum in the Intensity Curve

The intensity curves in Fig. 6 were obtained using X-rays and show, in distinction to the neutron curves of Fig. 2, a pronounced additional maximum at $q \cong 1.6$ Å^{-1} whose height is strongly concentration dependent and even higher than the main maximum at $q \cong 2.5$ Å^{-1} in the case of 20 and 30 at% Bi, respectively. This additional maximum is designed as premaximum. In the intensity-curves of Fig. 2, obtained by neutron diffraction, this feature is only indicated as a shoulder at the low q-part of the main maximum. The strongest indication is observed for the melt containing 40 at% Bi. Since up to now thin samples convenient for X-ray diffraction experiments could not be prepared from alloys containing more than 30 at% Bi, a comparison between X-ray and neutron structure factors $S^x(q)$ and $S^n(q)$ is done in Fig. 7 for the melt containing 30 at% Bi.

As suggested in [17] a premaximum can be described as modulation of the monotonic Laue scattering which is caused by short range order. In [18] a quantitative description was given on this subject, which finally resulted in the equation

$$S^{\mathrm{mod}}_{\mathrm{LMS}}(q) = c_{\mathrm{A}}\, c_{\mathrm{B}} \frac{(b_{\mathrm{A}} - b_{\mathrm{B}})^2}{\langle b \rangle^2} \cdot \left[\sum_{i=1} N^i \alpha^i \frac{\sin q\, r^i}{q\, r^i} \right]. \qquad (11)$$

In this equation, $S^{\mathrm{mod}}_{\mathrm{LMS}}(q)$ represents the contribution of the premaximum to the structure factor in Figure 7. r^i means the radius of the ith coordination sphere, which contains N^i atoms. The short range order is described by the short range order parameter α^i of the ith sphere (see [18]).

As can be seen from (12), the nature of the radiation used for a scattering experiment determines the amplitude of the modulation via the factor containing the scattering lengths.

According to [9] it can be shown that the heights of the premaxima near $q = 1.6$ Å^{-1} in the X-ray- and in the neutron-curve in Fig. 7 show a ratio corresponding to

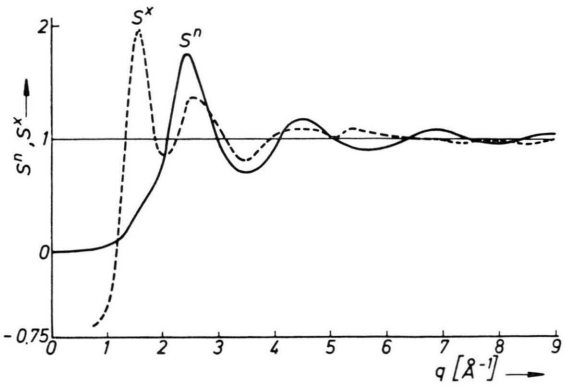

Fig. 7. Mg-Bi melt with 30 at% Bi: Total structure factors.

$$\frac{(b^{\mathrm{x}}_{\mathrm{A}} - b^{\mathrm{x}}_{\mathrm{B}})^2}{\langle b^x \rangle^2} \Big/ \frac{(b^{\mathrm{n}}_{\mathrm{A}} - b^{\mathrm{n}}_{\mathrm{B}})^2}{\langle b^n \rangle^2}.$$

This fact means indeed a proof for the correctness of the interpretation of these premaxima as being caused by the modulation of monotonic Laue scattering. Concerning the quantitative evaluation of the premaxima which leads to the determination of the short range order parameter for the melt containing 30 at% Bi, cf. [19].

5.3. Shoulder on the Main Maximum of the Intensity Curve

The intensity curve of pure molten Bi shows the run usually obtained for molten metals however with an additional shoulder on the high q-value side of the first maximum as frequently observed [15, 20, 21], which indicates the presence of Bi-tetrahedra in pure molten Bi [15]. The addition of Mg up to 20 at% yields no significant change in the shape of the intensity curves of Fig. 2 except a slight shift of the position of the first maximum to higher q-values. This shift is continued with rising Mg-content up to the value of pure Mg ($q = 2.43$ Å^{-1} according to [22]).

The intensity curve of the Mg-Bi melt with 70 at% Bi shows on the higher q side of the first maximum a broad shoulder the height of which rises compared to that of the first maximum with decreasing Bi-content. This shoulder is most pronounced for 40 at% Bi. From the concentration behaviour of the relative height of this shoulder it can be concluded that this shoulder is caused by another atomic configuration than the shoulder observed in the pure Bi-melt.

The shoulder under consideration does not occur in the structure factor curves of Fig. 7 obtained with the melt containing 30 at% Bi, but only seems to contribute to a certain broadening of the main maximum.

At the moment it is not possible to evaluate the origin of the shoulder, i.e. to decide whether the shoulder must be ascribed to the modulation of monotonic Laue scattering or not. Anyhow, from the fact, that the shoulder is most pronounced with the melt containing 40 at% Bi one can conclude that the shoulder is correlated with strong compound formation.

Further progress concerning this feature can be expected by performing X-ray experiments with a melt containing 40 at% Bi.

Thanks are due to the Kernforschungszentrum Karlsruhe for the allocation of beam time at the Research Reactor FR2.

[1] B. R. Ilschner and C. Wagner, Acta Met. **6**, 712 (1958).
[2] J. E. Enderby and E. W. Collings, J. Non Cryst. Solids **4**, 161 (1970).
[3] M. H. Cohen und J. Sak, J. Non Cryst. Solids **8–10**, 696 (1972).
[4] T. E. Faber, Introduction to the Theory of Liquid Metals, University Press, Cambridge 1972.
[5] R. W. James, The Optical Principles of X-Ray Diffraction, Bell, London 1958.
[6] H. Oehme, Dissertation, Universität Stuttgart 1968.
[7] W. Knoll and S. Steeb, Phys. Chem. Liq. **4**, 39 (1973).
[8] M. Hansen and K. Anderko, Constitution of Binary Alloys, McGraw-Hill, New York 1958.
[9] M. Weber, Diplomarbeit, Universität Stuttgart 1974.
[10] P. J. McGonigal, A. D. Kirshenbaum, and A. V. Grosse, J. Phys. Chem. **66**, 737 (1962).
[11] J. A. Cahill and A. D. Kirshenbaum, J. Inorg. Nucl. Chem. **25**, 501 (1963).
[12] R. C. Faxon, Ph. D. Thesis, Syracuse University 1966.
[13] A. Boos, S. Steeb, and D. Godel, Z. Naturforsch. **27a**, 271 (1971).
[14] S. Steeb and R. Hezel, Z. Metallkde. **57**, 374 (1966).
[15] P. Lamparter, W. Knoll, and S. Steeb, Z. Naturforsch. **31a**, 90 (1976).
[16] S. Steeb and R. Hezel, Z. Phys. **191**, 398 (1966).
[17] H. Ruppersberg and K. Goebbels, Z. Naturforsch. **27a**, 1018 (1972).
[18] A. Boos, P. Lamparter, and S. Steeb, Z. Naturforsch. **32a**, 1222 (1977).
[19] A. Boos and S. Steeb, Phys. Letters **63 A**, 333 (1977).
[20] D. M. North, J. E. Enderby, and P. A. Egelstaff, J. Phys. **C 1**, 1075 (1968).
[21] S. P. Isherwood and B. R. Orton, Phil. Mag. **17**, 561 (1968).
[22] S. Woerner, S. Steeb, and R. Hezel, Z. Metallkde. **56**, 682 (1965).